The role of thermal notch erosion in forcing localised calving failure and short-term increases in velocity at a lake-terminating glacier in southeast Iceland

Journal:	*Journal of Glaciology*
Manuscript ID	Draft
Manuscript Type:	Article
Date Submitted by the Author:	n/a
Complete List of Authors:	Baurley, Nathaniel; University of Southampton, Department of Geography and Environmental Science Hart, Jane; University of Southampton, Department of Geography and Environmental Science
Keywords:	Glacier calving, Ice velocity, Remote sensing, Glacier monitoring, Mountain glaciers
Abstract:	We utilised repeat high-resolution UAV-SfM surveys, alongside terrestrial photography acquired in-situ, to investigate, for the first time, the role of thermal notch erosion in forcing localised calving failure and subsequent short-term increases in velocity at a lake-terminating glacier. This data was acquired daily (where possible) across one week in July 2019 and two weeks in July 2021 to provide insights into a suite of processes that are presently under-studied. We demonstrate that high-magnitude calving (surface area >1000 m^2), occurring as a direct result of thermal notches at the waterline, can drive short-term increases in velocity up to 30% above the average, which are sustained for several days and occur over a much larger area of the glacier than was originally impacted by the initial calving event. We suggest that these findings present an important, yet previously undocumented aspect of the dynamic behaviour and overall stability of both freshwater and tidewater glaciers, warranting further research into these key processes.

The role of thermal notch erosion in forcing localised calving failure and short-term increases in velocity at a lake-terminating glacier in southeast Iceland

Nathaniel R. Baurley[1*] and Jane K. Hart[1]

[1]Geography and Environmental Science, University of Southampton, Southampton, United Kingdom.

***Correspondence:**
Nathaniel R. Baurley
n.baurley@soton.ac.uk

Keywords: thermal notch erosion, glacier calving, glacier velocity, uncrewed aerial vehicles, lake-terminating glaciers, glacier dynamics, structure from motion photogrammetry, glacier monitoring.

ABSTRACT

We utilised repeat high-resolution UAV-SfM surveys, alongside terrestrial photography acquired in-situ, to investigate, for the first time, the role of thermal notch erosion in forcing localised calving failure and subsequent short-term increases in velocity at a lake-terminating glacier. This data was acquired daily (where possible) across one week in July 2019 and two weeks in July 2021 to provide insights into a suite of processes that are presently under-studied. We demonstrate that high-magnitude calving (surface area >1000 m^2), occurring as a direct result of thermal notches at the waterline, can drive short-term increases in velocity up to 30% above the average, which are sustained for several days and occur over a much larger area of the glacier than was originally impacted by the initial calving event. We suggest that these findings present an important, yet previously undocumented aspect of the dynamic behaviour and overall stability of both freshwater and tidewater glaciers, warranting further research into these key processes.

1. INTRODUCTION

Frontal ablation, or the loss of ice from the termini of calving glaciers, occurs by a combination of "mechanical" iceberg calving and subaqueous melt (Truffer and Motyka, 2016; How and others, 2019; Carrivick and others, 2020). Mechanical calving can occur via four mechanisms: (i) longitudinal stretching; (ii) stresses associated with force imbalances at the ice front; (iii) melt undercutting of the ice front; and (iv) torque arising from buoyant forces (Benn and others, 2007). Subaqueous melt, meanwhile, in addition to melting the terminus face directly, can further enhance mechanical calving by undercutting and destabilising the subaerial portion of the glacier front (O'Leary and Christoffersen, 2013; Luckman and others, 2015; How and others, 2019).

The process of subaqueous melt, and specifically melt undercutting, plays an important role in controlling both the calving rate and overall stability of calving glaciers in both freshwater and tidewater settings (Luckman and others, 2015; Truffer and Motyka, 2016; Benn and Åström, 2018). Indeed, it is now recognised as a highly significant process, particularly in those environments where relatively warm water is brought into contact with glacier termini, including fjords in Alaska, Svalbard and Greenland, and lakes in Patagonia and New Zealand (e.g., Dykes and others, 2011; Bartholomaus and others, 2013; Rignot and others, 2015; Minowa and others, 2017; Schild and others, 2018). In these settings, melt is a function of the water temperature and the tangential movement of this water across the ice front, which ensures efficient energy transfer (Jenkins and others, 2011; Pętlicki and others, 2015; Benn and Åström, 2018).

As such, whenever melt rates at the waterline exceed those above, the calving front will be progressively undercut, leaving the subaerial portion of the terminus overhanging a sub-horizontal waterline notch, resulting in an increase in force imbalance at these locations (Röhl, 2006; Benn and others, 2007; Pętlicki and others, 2015). Calving can then occur along preferential lines of weakness (e.g., surface crevasses), either as low magnitude events where undercuts are small, resulting in localised, shallow subaerial failures, or as high magnitude events where undercuts are large, resulting in the collapse of the entire ice column (Benn and others, 2007; 2017; Mallalieu and others, 2020). For those glaciers where melt undercutting is the primary control on calving, whether they calve via low or high magnitude events will have important implications for the long-term calving rate, and consequently, the dynamic behaviour and overall stability of these glaciers across different spatial and temporal scales (O'Leary and Christoffersen, 2013; How and others, 2019).

Indeed, there is the potential that these high magnitude events could even drive short-term variations in ice dynamics, with observations from several tidewater glaciers in Greenland suggesting that particularly large calving events (which are not necessarily forced by melt undercutting) can result in an acceleration of ice flow that is sustained long after the initial event occurred (Nick and others, 2009; Howat and others, 2010; Murray and others, 2015). Yet although speed-ups in response to undercut-driven calving are yet to be observed in nature, the clear potential for such events to occur raises important implications for the dynamics and overall stability of these glaciers. However, while further work is required in order to better understand these processes, most studies over recent years have predominately been undertaken in tidewater environments, particularly in Svalbard and Greenland (e.g., Luckman and others, 2015; Rignot and others, 2015; Jouvet and others, 2018; Schild and others, 2018).

In contrast, while melt undercutting and notch erosion have been known to be important drivers of calving losses in freshwater environments for over two decades (e.g., Kirkbride and Warren, 1997; Haresign and Warren, 2005; Röhl, 2006), since this time the number of studies has been severely limited (e.g., Mallalieu and others, 2017; Minowa and others, 2017). Most recently, Mallalieu and others (2020) were able to provide the first continuous year-round record of calving processes in a freshwater setting by using an integrated time-lapse and structure from motion (SfM) approach, identifying two distinct calving regimes which they relate to melt undercutting and variations in lake ice. In general, however, a lack of quantitative data relating to calving processes and their associated drivers means these processes are not well understood (Purdie and others, 2016; Mallalieu and others, 2020). Furthermore, no study (to the best of our knowledge) has investigated the role that undercut-driven calving may have on forcing short-term increases in velocity, specifically in freshwater settings, despite the potential for such a process to result in increased mass loss across different scales. As such, the relative importance of these processes in forcing the dynamics and overall stability of freshwater calving glaciers remains difficult to assess.

Uncrewed aerial vehicles (UAVs) may provide new opportunities and insights, however, due to their ability to offer rapid repeat assessments of glacier surface dynamics at extremely high spatial (cm-scale) and temporal (sub-daily) resolutions (Whitehead and others, 2013; Ryan and others, 2015; Chudley and others, 2019). Indeed, when combined with modern and relatively low-cost SfM techniques, the method can be used to generate detailed orthomosaics and DEMs of the ice surface and surrounding morphology, from which a number of different glacier-specific products can be derived with relatively low error (e.g., Immerzeel and others, 2014; Wigmore and Mark, 2017; Bash and others, 2018; Yang and others, 2020). The UAV-SfM approach has previously been used to investigate the velocity of calving glaciers (e.g., Ryan and others, 2015; Jouvet and others, 2019) as well as their calving dynamics (e.g., Jouvet and others, 2017, 2019), however, the influence of calving on forcing short-term speed-up events, driven by melt-undercutting at the waterline, has yet to be assessed using this method, providing scope for its deployment here.

Consequently, in this study we utilise repeat high-resolution UAV-SfM surveys, alongside terrestrial photography acquired in-situ, to investigate the role of thermal notch erosion in forcing localised calving failure and subsequent short-term increases in velocity at an actively calving lake-terminating glacier in southeast Iceland. More specifically, we aim to (i) quantify how thermal notches develop and evolve at the waterline over time; (ii) evaluate how high magnitude calving events are directly controlled by the presence of extensive waterline notches; and (iii) demonstrate how large calving events subsequently drive short-term increases in velocity across different spatial and temporal scales. The findings of this study present an important and previously undocumented aspect of calving glacier behaviour, which has the potential to occur in both freshwater and tidewater settings. Consequently, we suggest future work should investigate the relative importance of these processes for other calving glaciers in similar settings, in order to better understand their current dynamic behaviour and overall stability.

2. STUDY AREA

Fjallsjökull (64°01′N, 16°25′W) is a large lake-terminating glacier situated on the southern side of the Vatnajökull Ice Cap, in southeast Iceland (Fig. 1) (Evans and Twigg, 2002; Dell and others, 2019). The glacier has an area and length of ~44.6 km^2 and ~12.9 km, respectively, and like many glaciers in Iceland has undergone significant recession over the last century, particularly since the early 2000s (Hannesdóttir and others, 2015; Guðmundsson and others, 2019). This ongoing retreat has led to the emergence of a substantial overdeepening (~206 m deep, ~3 km wide and ~4 km long), resulting in the development of the large proglacial lake Fjallsárlón (~3.7 km^2) into which the glacier currently terminates (Magnússon and others, 2012; Guðmundsson and others, 2019).

Recent research by Dell and others (2019) has indicated that the deep subglacial topography and continued expansion of Fjallsárlón have become important controls for the overall dynamics of the glacier, particularly over recent decades. The authors also suggest that calving at Fjallsjökull likely occurs by a combination of buoyant forces acting on the terminus, melt undercutting and force imbalances at terminal ice cliffs, particularly in those locations where the bed topography is deepest, although they were unable to provide direct evidence for any these processes occurring. As such, the role of melt undercutting (i.e., thermal notch erosion) as a control on calving activity and subsequent short-term velocity increases remains poorly understood.

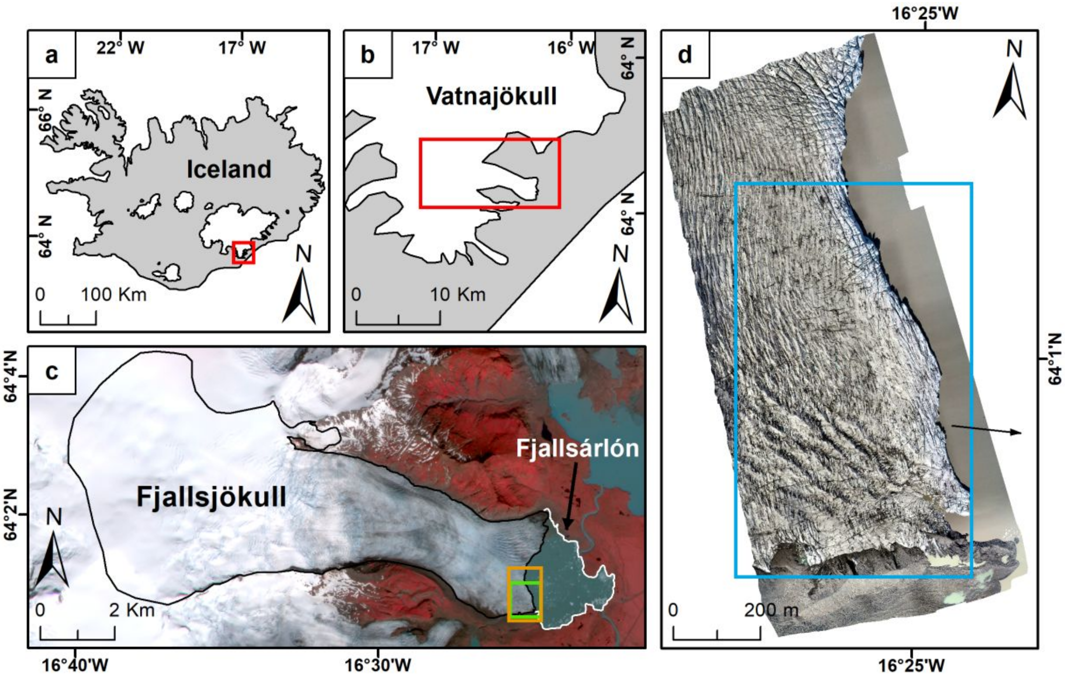

Fig. 1. Location map of Fjallsjökull. Location of Fjallsjökull within Iceland, and (b) within the Vatnajökull Ice Cap. (c) Area of Fjallsjökull and Fjallsárlón as of July 2021. Glacier outline obtained from the GLIMS database, with the green and orange boxes delineating the areal coverage of the UAV-SfM surveys undertaken in 2019 and 2021, respectively. These also reflect the glacier extents shown in Figs. 2a, 2b. Background is a 4-band false-colour PlanetScope acquisition from 7 July 2021. (d) UAV orthomosaic from 7 July 2021, with the blue box illustrating the areal extent over which the analyses presented in this study are focused. Black arrow indicates the average ice flow direction of this region.

3. DATA AND METHODS

3.1. Repeat UAV-SfM Surveys

UAV-SfM surveys at Fjallsjökull were conducted over five days in early July 2019, and across 11 days in July 2021. These surveys were undertaken using two different UAV systems: a 3DR Solo quadcopter (2019) and a DJI Inspire 2 (2021). The technical specifications of both UAV systems, and the specific camera settings used, are given in Tables S1 and S2. For both years, all surveys were pre-designed using parallel flight lines placed orthogonal to ice flow direction, with full coverage of the study region obtained by undertaking multiple flights, ensuring sufficient inclusion of stable ground areas adjacent to the glacier terminus for use in the uncertainty assessment (Figs. 2a, 2b). All surveys were then flown autonomously at a constant elevation, resulting in a GSD of 0.03 m for both the 2019 and 2021 surveys. Key flight parameters from both years are shown in Table 1, while specific details of each individual survey, including dates, number of flights and the number of photos captured, are given in Table S3.

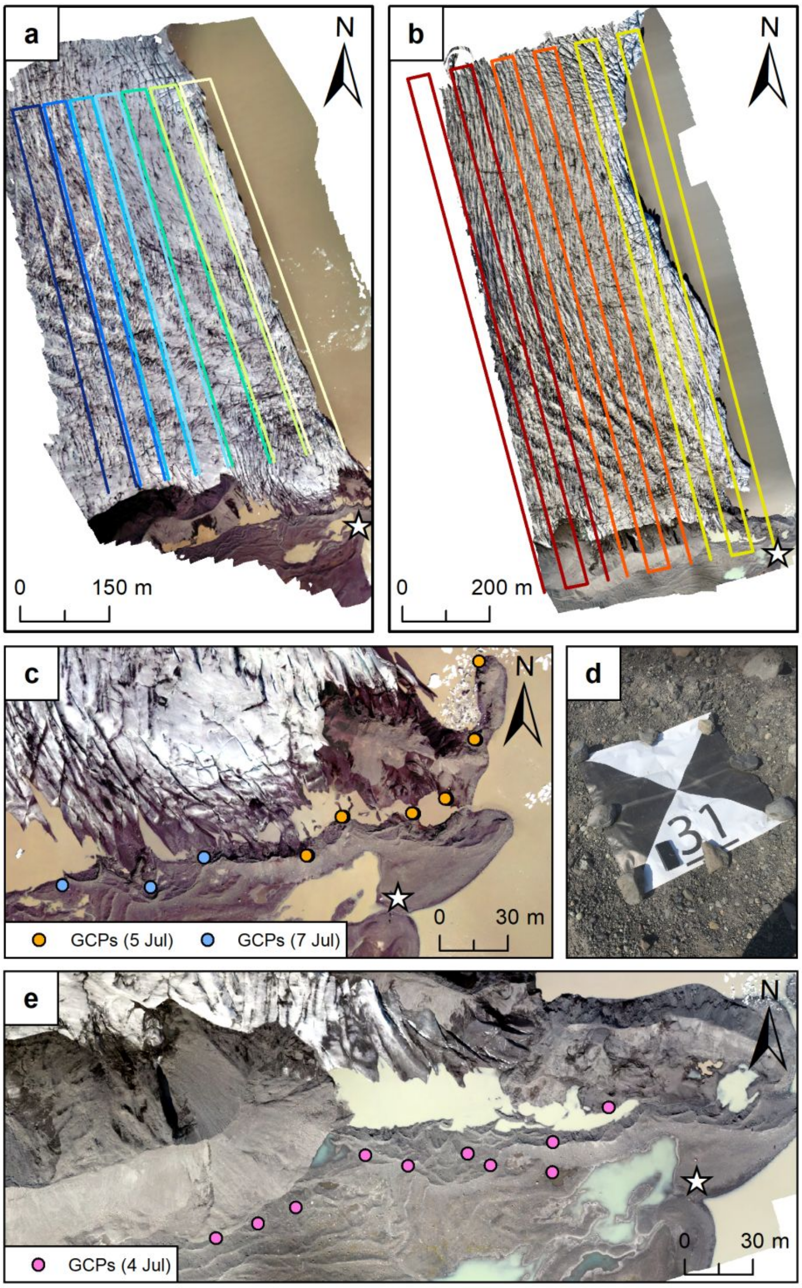

Fig. 2. Areal coverage of the UAV-SfM surveys flown over the study region in (a) 2019 and (b) 2021. Each individual flight is shown in a different colour. (c) GCP locations on 5 and 7 July 2019. All GCPs were resurveyed, and three more added on 7 July due to the loss of the northernmost GCP between 6 and 7 July. (d) Example of one of the GCPs used in this study. (e) GCP locations on 4 July 2021. The white star in (a)-(c) and (e) signifies the take-off and landing point in that year. Background in (a) & (c) and (b) & (e) is the UAV-SfM orthomosaic from 7 July 2019, and 7 July 2021, respectively.

To accurately georeference the 2019 imagery, a set of ground control points (GCPs) were deployed across stable ground near the lateral margin of the glacier, ensuring good spread in the X, Y and Z planes (Fig. 2c). The GCPs used here were high contrast, thick plastic markers, 1x1 m in size, with a clearly defined centroid to aid in locating the target centre during processing (Fig. 2d), with the centre position of each GCP recorded in the field using a Leica GS09 dGPS with an accuracy of <0.01 m. Seven GCPs were originally deployed around the study site at the start of fieldwork on 5 July 2019, although this was then increased to nine markers two days later.

Table 1. Flight parameters when undertaking the 2019 and 2021 UAV-SfM surveys.

Flight Parameters	2019	2021
Areal coverage (km^2)	0.511	0.858
UAV flying height AGL (m)	80	90
UAV flying speed ($m\ s^{-1}$)	5.0	7.5
Image Overlap	90%	80%
Image Sidelap	70%	70%
GSD (m)	0.03	0.03

In contrast, due to the on-board differential carrier-phase GNSS functionality of the DJI Inspire 2, the 2021 imagery were instead accurately georeferenced using a PPK method after Tomsett and Leyland (2021) and Baurley and others (2022). This resulted in post-processed camera locations accurate to <0.05 m. However, a small network of ten GCPs were still deployed across the study site for redundancy (Fig. 2e). These were the same markers used in 2019, with the centre position of each GCP recorded using a Leica GS15 dGPS to <0.01 m. Although it was intended that all UAV-SfM imagery from 2021 would be processed using the PPK method, a technical problem on 15 July meant no positional or timestamp data were recorded, and as such the images acquired from this day were georeferenced using the GCPs.

3.2. 3D Model Generation (SfM Photogrammetry)

All images from each survey were processed using an SfM workflow (e.g., Westoby and others, 2012) in Agisoft Metashape Professional v. 1.7 (Agisoft LLC, 2021). First, each image set was imported into Metashape, along with the relevant GCP and camera locations. An alignment procedure was then undertaken, based off the positional information of either the GCP locations (2019), or the post-processed camera locations (2021), resulting in georeferenced spare point clouds. The only exception was for those surveys undertaken on 15 July 2021, where the alignment procedure was undertaken using the GCP locations recorded in the field. Following this, an optimisation procedure was performed in order to remove non-linear deformations and georeferencing errors from the final models (Agisoft LLC, 2021). Dense point clouds were then generated, from which DEMs and orthomosaics for each survey day were produced, with these exported from Metashape at resolutions of 0.07 and 0.03 m (2019), and 0.05 and 0.03 m (2021), respectively, for further analysis.

3.3. Uncertainty Assessment

The relative uncertainty of the generated 3D models from both 2019 and 2021 were assessed by undertaking a repeat assessment of stable ground topography, following the method of Tomsett and Leyland (2021) and Baurley and others (2022). This follows the principle that stable ground should be consistent between surveys and, therefore, any variations are indicative of the uncertainty in the system (e.g., Chudley and others, 2019; Yang and others, 2020). This in turn affects the level of confidence in the data and the level of change that can be detected. Indeed, because an extensive ground control network could not be deployed in either 2019 or 2021 due to the relative inaccessibility of the glacier surface, this stable ground assessment was essential to identify any errors between the generated 3D models.

For this assessment, an area of ice-free stable ground near the lateral margin of the glacier was selected that encompassed both shallow and steep topography and which was present in all the generated dense point clouds. This region was then extracted from each individual point cloud simultaneously to avoid any potential differences in stable ground extent. Once selected, each point cloud was differenced to each of the others in a pairwise fashion within CloudCompare v. 2.11.3, using the M3C2 algorithm developed by Lague and others (2013). This allowed the error to be assessed by comparing the median error, the Normalised Median Absolute Deviation (NMAD), as well as visualising their distribution, as outlined by Höhle and Höhle (2009). These errors could then be used to identify the minimum change detection threshold between surveys, which ensured that any differences present in the point clouds (and thus resultant DEMs and orthomosaics) represented actual change.

3.4. Observations of Thermal Notch Formation and Evolution

To investigate the presence and evolution of thermal notches across our study region, repeat digital photographs of the calving front were acquired daily in both 2019 and 2021 using a Nikon D3300 DSLR camera. Where possible, images were captured from the same location (by using stone markers in the field) and at the same time of day (11:00) to ensure the captured scene did not vary significantly between the different days. Note this location was different in 2019 and 2021 due to recession of the ice margin. No image was captured on the 5 July 2019 due to a technical issue with the camera, so the image acquired on the 4 July was used in subsequent analyses. These photographs were then examined to determine the spatio-temporal distribution of thermal notches, as well as their specific morphology.

3.5. Variations in Frontal Position and Calving Events

To assess changes in calving front geometry and evolution, the position of the terminus in each orthomosaic was manually digitised in ArcGIS at a scale of 1:30. To estimate the location and area of ice that calved between two repeat flights, DEM differentiation was utilised, whereby the earlier DEM was subtracted from the latter DEM to retrieve a spatially distributed map of change. The location and area of each individual calving event was then manually digitised in ArcGIS, with the corresponding differenced DEM used to define the horizontal extent of each event. The uncertainty in both approaches was quantified through repeat digitisation techniques (at a scale of 1:30), before calculating the standard error for each time period (after Baurley and others, 2020).

3.6. Localised Velocity Variations

To derive high-resolution velocity fields, the free software CIAS was utilised (https://www.mn.uio.no/geo/english/research/projects/icemass/cias/), which allows glacier surface displacements to be calculated with sub-pixel accuracy (Haug and others, 2010; Heid and Kääb, 2012). Prior to processing, each orthomosaic was first resampled to a resolution of 0.25 m, before georeferencing each orthomosaic pair in ArcGIS. Depending on the temporal separation between successive orthomosaics, the specific processing parameters varied, with these given in Table S4. The resulting displacements were then filtered by direction and magnitude, following a similar approach to Robson and others (2018), before being interpolated using ordinary kriging to produce velocity fields for each period.

To determine the uncertainty of these calculations, displacements were measured over areas of stable ground that contained variable surface topography (Fig. S1.) (e.g., Chudley and others, 2019; Jouvet and others, 2019). This analysis was undertaken over three distinct zones close to the glacier margin that were covered by both the 2019 and 2021 surveys, before calculating the combined stochastic standard deviation. Stable ground locations were chosen as theoretically no change should have occurred in these locations, and as such, they provide a good estimation for the accuracy of the velocity calculations.

4. RESULTS

The analyses presented in Sections 4.2.- 4.4., and the discussion that follows, will focus solely on the lower region of the study area illustrated in Fig. 1d. This is because field observations from both 2019 and 2021 indicate that thermal notches (and related calving activity and speed-up events) predominately occur in this region, and, therefore, it is of most interest due to the specific aims of this study.

4.1. Uncertainty Assessment

The results of the stable ground assessment importantly display similar levels of consistency between the different surveys from both 2019 and 2021. For the July 2019 comparisons (Fig. S2), the median error between points was between -0.045 and 0.069 m (1.5-2.3 GSD), with NMAD values no greater than ±0.227 and as low as ±0.097 m. Similarly, for the July 2021 comparisons (Fig. S3) the median error was between 0.04 and -0.099 m (~1.3-3.3 GSD), with NMAD values of between ±0.04 and ±0.26 m. As a result, these errors indicate that in both years the difference between stable ground locations were small.

These errors also show very good agreement with those previous studies within glaciology that have undertaken their own UAV-SfM surveys at similar flying heights to those undertaken here. Across these studies, the range of reported errors was between 1.5 and ~3 times the GSD, with the flying heights of each respective survey ranging between 90 m and 110 m (e.g., Ely and others, 2017; Wigmore and Mark, 2017; Bash and others, 2018; Rossini and others, 2018; Xue and others, 2021). Overall, the results of the uncertainty assessment indicate that the errors found for all surveys across both years are smaller than the change expected over each period of interest (decimetre-metre scale) and are thus well within the realm of acceptability.

4.2. Observations of Thermal Notch Formation and Evolution

A comparison of the calving front at the beginning and end of fieldwork in both 2019 and 2021 clearly indicates that thermal notches are present in this region of Fjallsjökull, and that their relative extents develop and evolve over time (Fig. 3). In general, the notches are more extensive (both vertically and horizontally) at the beginning of each study period, with their morphology showing a clear stepped pattern which reverses back towards the lake. This is particularly noticeable at the beginning of fieldwork in 2019 and may indicate that the level of the lake dropped since the notches were first formed in order for the stepped pattern to be visible. In contrast, by the end of the study period these notches are less extensive and morphologically less distinct, showing no stepped pattern, and with only a small reverse slope visible at the end of fieldwork in 2019, not in 2021.

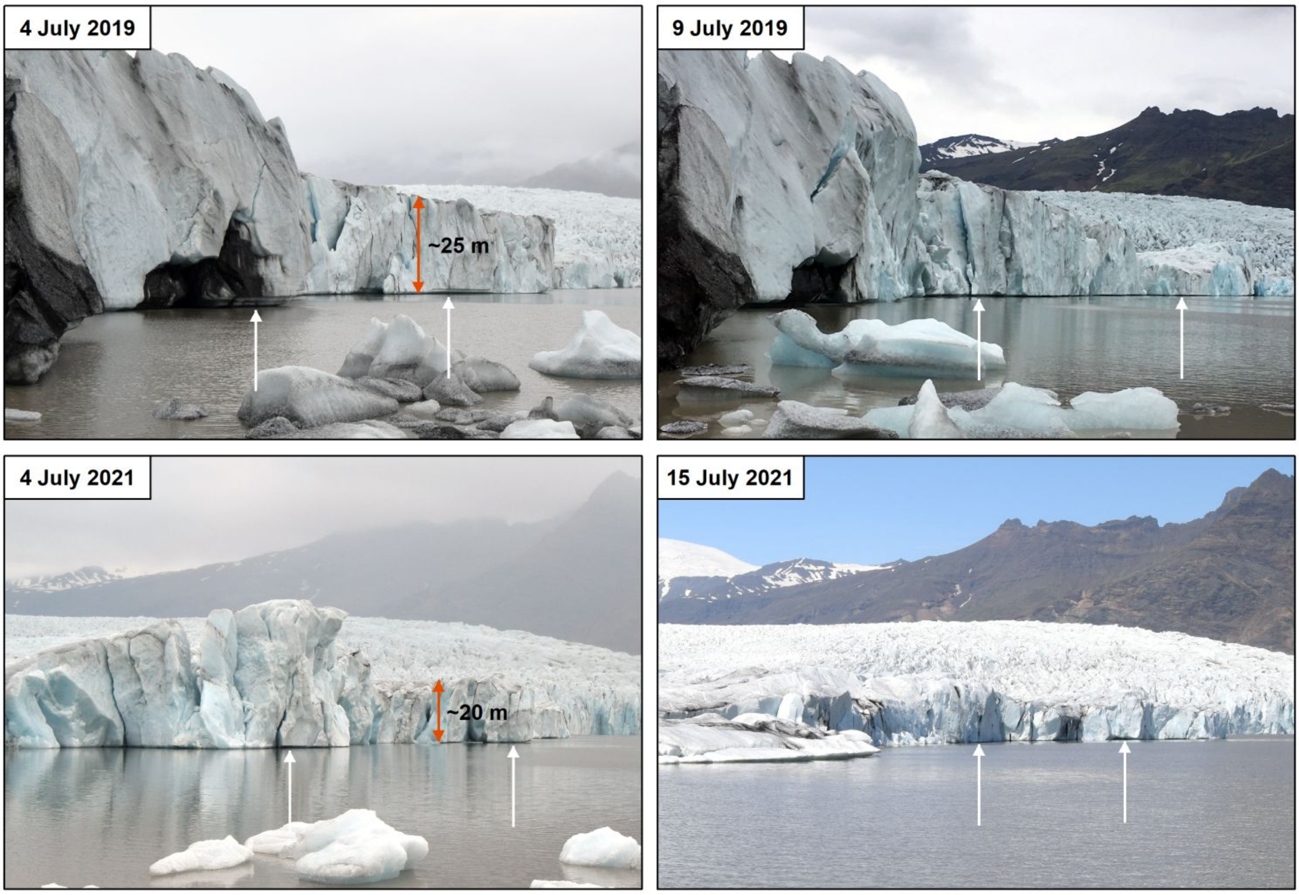

Fig. 3. Photographs comparing the relative extent of thermal notches at the beginning and end of fieldwork in 2019 (top) and 2021 (bottom). Locations of notches in each photo are denoted by the white arrows. Height of the calving front in 2019 and 2021 is estimated from the generated DEMs from each year. As no image was captured on 5 July 2019, the image acquired on the 4 July was instead used in this analysis to mark the beginning of fieldwork.

Furthermore, the complete time series of observations also reveals distinct daily variations in the relative extent of these thermal notches (Figs. S4, S5), particularly from those images captured in 2021. For example, between the 4 and 7 July, the notches become steadily less extensive, so that by the 8 July almost no notches are visible in this region of the calving front. However, over the following few days a new set of notches can be observed forming at the waterline, so that by the end of the study period relatively extensive thermal notches are once again present, with a similar pattern also observed in the 2019 time series. Such a pattern likely reflects the occurrence of large calving events in this region, which have the effect of removing the notched portion of the terminus, causing the process of notch formation to reset.

It is important to note that although no direct measurements of notch erosion could be made here, the fact they are present in nearly every photo, and in some cases very extensive, suggests the rates of notch erosion must be significant. Indeed, by using the produced DEMs we are able to estimate that the calving front in this region is ~25 m (2019) and ~20 m (2021) high, which based on the time series of imagery suggests that notches reaching up to at least ~0.5 m in vertical extent are not inconceivable.

4.3. Variations in Frontal Position and Calving Events

In general, the position of the calving front remained relatively stable across all time periods in both 2019 and 2021, with only a small number of significant changes in calving front geometry (i.e. large calving events) occurring during this time (Fig. 4). Indeed, in both years calving is dominated by a high number of low-magnitude events (<100 m^2) (Table S5), with an average size of 55.63 m^2 and 233.06 m^2 in 2019 and 2021, respectively. As a result, the greatest changes in frontal position occur as a direct result of only three large (>1000 m^2) calving events: one in 2019, and two in 2021 (Figs. 4c-e).

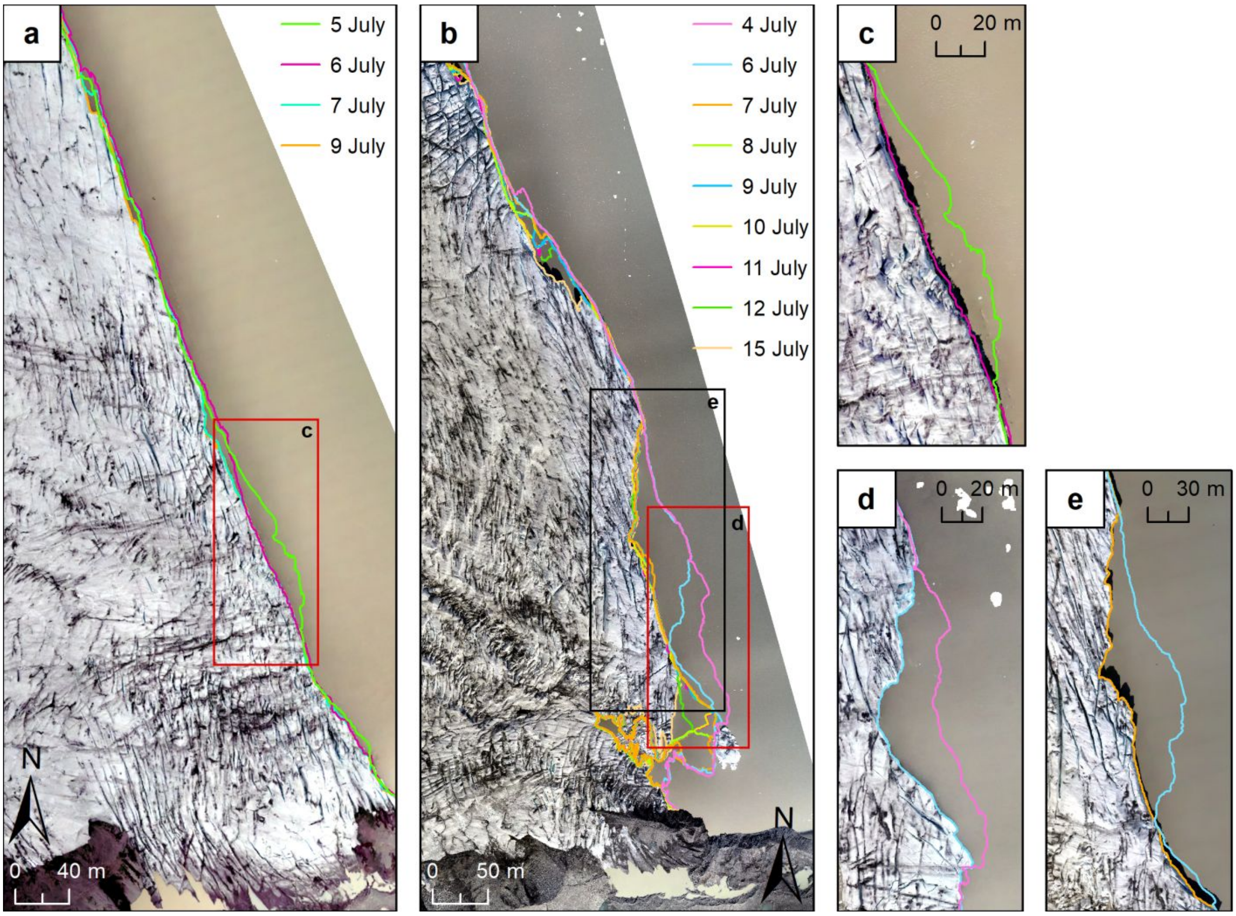

Fig. 4. Change in calving front position between the (a) 5-9 July 2019 and (b) 4-15 July 2021. The boxes in (a) and (b) indicate where the large calving events occurred in both years, with these presented in panels (c)-(e). The corresponding dates for these events are: (c) 5-6 July 2019, (d) 4-6 July 2021, and (e) 6-7 July 2021. See main text for more detail on each individual event. Background in each panel is the orthomosaic for the latest period.

The large calving event observed in 2019 occurred in the lower portion of the study region between the 5 and 6 July. The event was approximately 150 m by 20 m (at its widest point) and resulted in ~1,579.05 m^2 of ice being lost, which is ~28 times larger than the average for this period. Similarly, the two large calving events that were observed in 2021 also occurred in the lower portion of the study region. The first of these events occurred between the 4 and 6 July, was approximately 155 m by 30 m (at its widest point) and resulted in ~2,948.62 m^2 of ice being lost, which is ~12 times larger than the average for this period. The second event occurred between the 6 and 7, in the exact same region as the first, but over a much greater extent, being approximately 200 m by ~55 m (at its widest point). This resulted in ~4,629.84 m^2 of ice being lost, which is ~1.5 times larger than the first event, and ~20 times greater than the average for this period. Importantly, while these large events are infrequent, only representing ~1-2% of the total calving activity across both years, their contribution to overall mass loss is significant, accounting for ~40% of the total area lost through calving in both 2019 and 2021.

It is important to note that the calculated standard error for both sets of analyses was <1% for all time periods in both years, indicating that the calculated uncertainty was not greater than the change observed during this time.

4.4. Localised Velocity Variations

The velocity results (Fig. 5) demonstrate an overall pattern, whereby velocities increase with increasing distance from the southern-grounded margin. However, within this overall pattern, smaller-scale, more localised velocity variations, which occur over several days, can also be observed. For example, localised increases in velocity (i.e., speed-up events) occur between both the 5 and 9 July 2019, and the 4 and 11 July 2021, with these variations seemingly closely related to the occurrence of the large calving events described previously. Therefore, to assess the influence of these events on the ice velocity, for each period flow transects (shown in Fig. 5) were extracted from the middle of where each calving event occurred back into the ice interior. These results are shown in Fig. 6.

The 2019 speed-up event was initially only limited to the region immediately surrounding where the large calving event occurred, with velocities reaching a peak of ~0.84 m d^{-1} by the 6 July, which is ~20% faster than the average. A further increase in velocity was observed over the following 24-hour period, reaching an event peak of ~0.88 m d^{-1} (~5% faster than the previous 24 hours), while the areal extent of this region of elevated velocities also increased in this period. By the 9 July, despite peak velocities decreasing slightly to ~0.86 m d^{-1}, much of the region behind the calving front and into the glacier interior was still flowing at elevated velocities, ~12% faster than at the onset of the speed-up event. Furthermore, although no UAV surveys were undertaken after the 9 July, it is likely that over the following 24-48 hours velocities in this region once again returned to their pre-event magnitude.

The 2021 speed-up event, like in 2019, was initially only limited to the region surrounding where the first large calving event occurred, with velocities peaking at ~0.72 m d^{-1} by the 6 July, which is 15% faster than the average. In contrast to 2019, however, following the occurrence of the second large calving event between the 6 and 7 July, velocities continued to increase over the following 48 hours, only reaching the event peak of ~0.94 m d^{-1} by the 9 July. This is ~30% faster than the velocity observed at the onset of the event. Furthermore, the areal extent of this region of elevated velocities also increased in this period, again reaching its maximum by the 9 July. After this point, however, velocities begin to decrease, so that by the 11 July they have returned to a similar distribution and magnitude as was observed ~five days earlier, marking the cessation of the speed-up event.

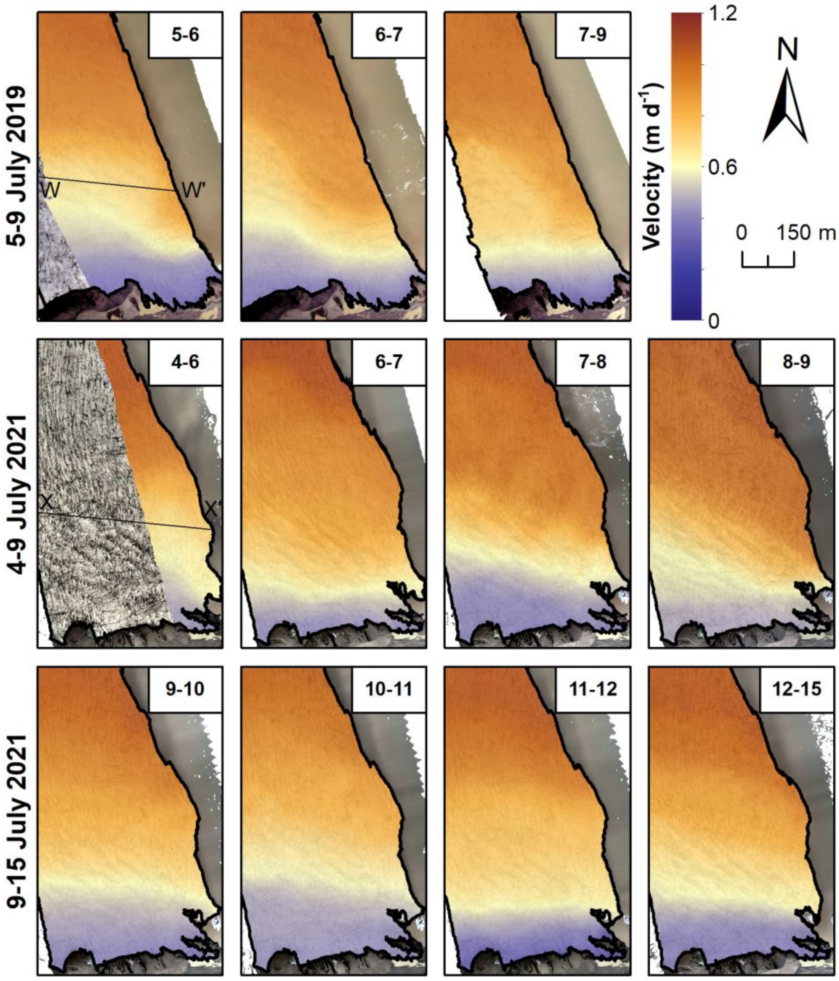

Fig. 5. Horizontal velocity fields for all time periods, calculated using feature tracking on UAV-derived orthomosaics. Lines W-W' and X-X' denote the beginning and end, respectively, of the flowlines used to extract the velocity profiles presented in Fig. 6. Average ice flow direction in this region is shown in Fig. 1d. Background in each panel is the orthomosaic for the latter period.

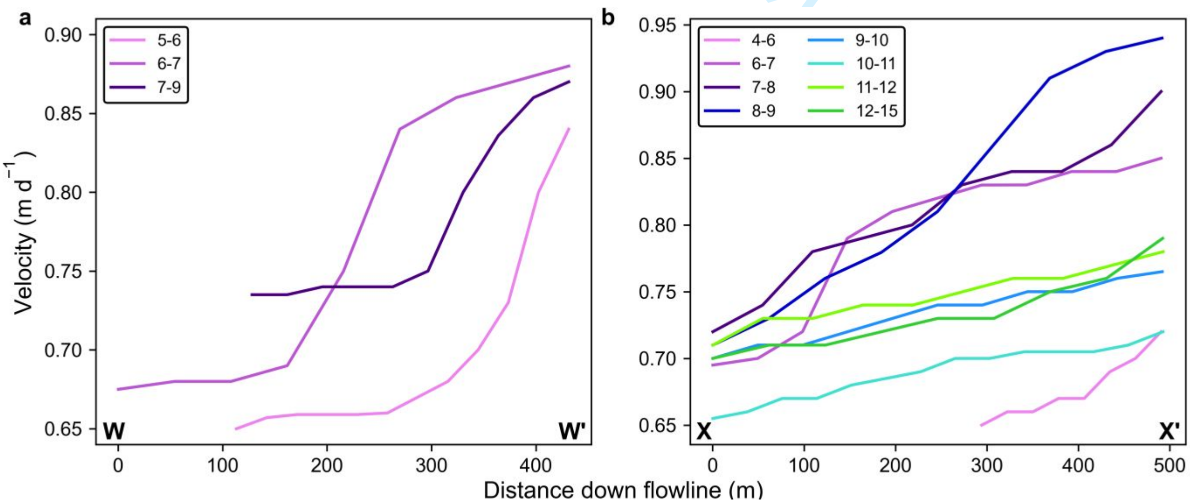

Fig. 6. Velocity profiles for all time periods in (a) 2019 and (b) 2021, generated by extracting the flowlines W-W' and X-X' from the relevant UAV-derived velocity fields shown in Fig. 5.

It is important to note that during these events, the region of elevated velocities extended some several hundred metres back into the interior of the glacier, encompassing a much larger area than was originally influenced by the initial calving events, with these regions of elevated velocities also sustained for several days after these events occurred (Figs. 5, 6). Finally, following the stable ground accuracy assessment, the combined stochastic standard deviation for this analysis was ±0.10 m d^{-1} and ±0.11 m d^{-1} in 2019 and 2021 respectively, which only represents ~11% of the total ice motion in both years.

5. DISCUSSION

5.1. Formation and Evolution of Thermal Notches at Fjallsjökull

Thermal erosion notches have previously been reported at other lake-terminating glaciers in several regions, including New Zealand (e.g., Röhl, 2006; Dykes and others, 2011), Patagonia (e.g., Haresign and Warren, 2005; Minowa and others, 2017) and Greenland (e.g., Mallalieu and others, 2020). In these settings, notch formation is often controlled by a combination of several factors, including water temperature, wind-driven wave action, ice cliff geometry and water-level fluctuations (e.g., Röhl, 2006; Truffer and Motyka, 2016; Minowa and others, 2017). Although notch formation can also be driven in some regions by melt-driven circulation, such as for those glaciers on the eastern side of the Southern Patagonian Ice Field, in most freshwater settings its influence is limited due to cooler lake temperatures, and consequently reduced mixing (Truffer and Motyka, 2016).

Of these factors, it is how much the level of the water body fluctuates that is often considered a key driver of notch formation in freshwater environments (Benn and others, 2007; Mallalieu and others, 2020). Indeed, observations by Röhl (2006) found that notch development was most efficient when water levels remained relatively constant, as this allowed the heat energy from the surface water to be concentrated in a narrower band of ice. In contrast, a rapid rise in lake level is likely to inhibit notch formation as this forces the melt to be dissipated over a larger elevation range (e.g., Mallalieu and others, 2020). However, very few measurements of notch melting at lake-margins have been made, although rates of between 0.2 and 0.3 m d^{-1} were recorded at Miage (Diolaiuti and others, 2006) and Tasman (Röhl, 2006) glaciers, while rates of 0.8 m d^{-1} were reported by Haresign and Warren (2005) at Glacier Leon. More recently, it has been suggested that such rates of notch erosion may be occurring at the termini of Glaciar Perito Moreno, Patagonia (Minowa and others, 2017) and Russel Glacier, Greenland (Mallalieu and others, 2020), although neither study were able to provide direct measurements.

At Fjallsjökull, thermal notch formation is likely driven by a combination of relatively warm surface water and variations in water-level, with the largest, most extensive notches forming when the water-level remains relatively constant. Indeed, because the observed notches in both 2019 and 2021 were extensive, particularly in depth (Figs. 3, S4 and S5), suggests that the level of Fjallsárlón must have remained relatively consistent across both periods, permitting significant amounts of thermal melt to occur. Furthermore, additional evidence for this is provided in both years through the repeat terrestrial photographs of the calving front, which have allowed the formation and growth of new thermal notches to be directly observed.

For example, in 2021, although notch formation had been reset following two large calving events between the 4 and 7 July, less than 24 hours later, small notches could once again be observed at the waterline, with these continuing to grow and develop over the following four days (Fig. 7). As a result, by the 12 July these notches were once again as extensive (both in size, as well as in area covered) as those first observed on the 4 July, before the large calving events had occurred. A similar pattern of notch re-formation and growth following calving was also observed in July 2019 (Fig. S4). These observations are important, not only because they confirm that notch erosion is actively occurring, but also because they indicate that the *rate* of notch erosion must be significant to allow these features to form and grow at the waterline of Fjallsjökull in such a short period of time.

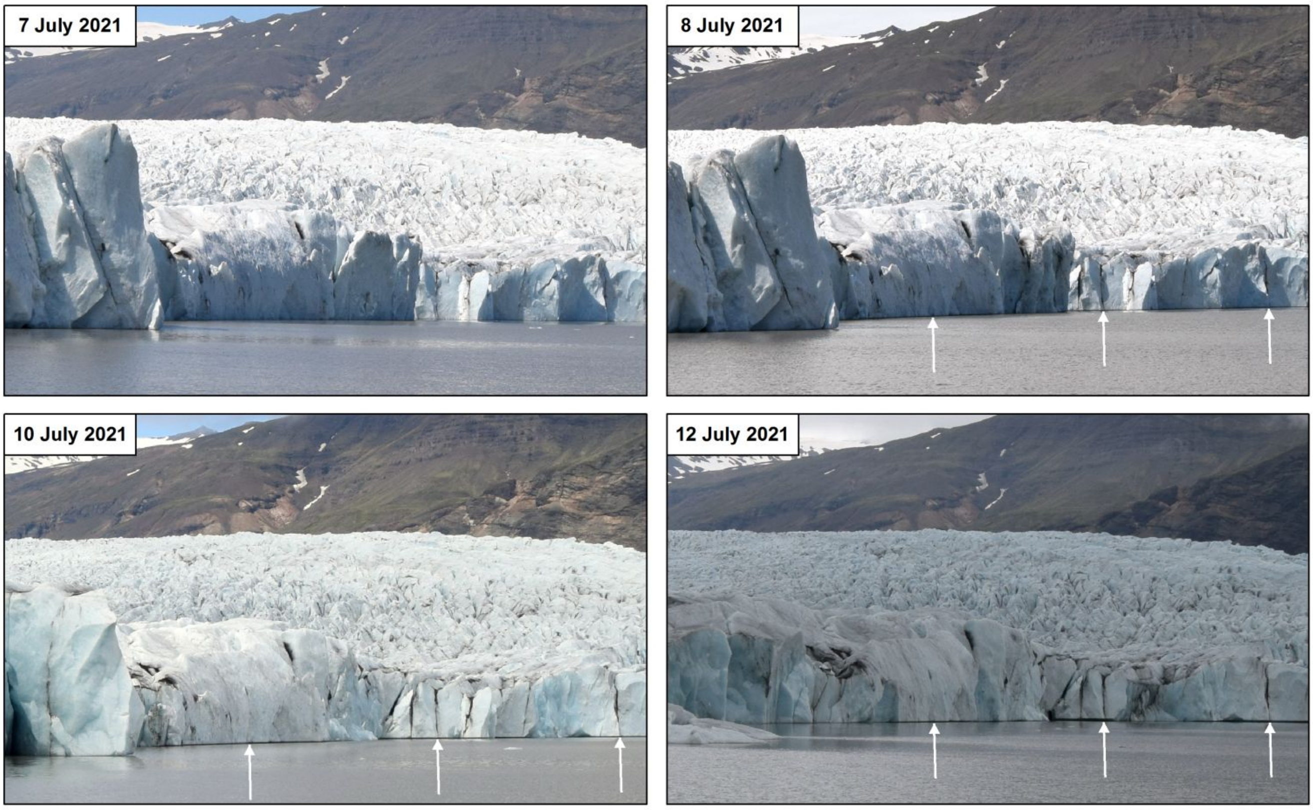

Fig. 7. Photographs illustrating the formation and growth of thermal notches for select dates between the 7 July (when no notches were observed) and the 12 July 2021 (when extensive notches are once again observed). White arrows denote the location of the new notches which formed and grew at the waterline in this five-day period. For reference the calving front here is ~20 m high.

As in several previous studies, no direct measurements of notch erosion could be made here, but the fact these notches formed and evolved so rapidly means it is not inconceivable that rates of ~0.5 m d^{-1} may have been occurring in this region of Fjallsjökull in both years. Such rates could only have occurred, however, if the water level of Fjallsárlón remained relatively consistent, as this would have allowed the heat energy from the lake surface to be more efficiently concentrated in a narrower band of ice (e.g., Röhl, 2006). Unfortunately, no physical measurements of lake level could be obtained in this study either, but direct observations made in the field (Figs. S4, S5) indicates that the level of the lake fluctuated very little during either period, which would have allowed such rates of notch erosion to occur. To our knowledge, this is one of the first studies to directly observe the formation and growth of new thermal notches at the waterline of a lake-terminating glacier following the occurrence of large calving events. As a result, these observations may be important for our understanding of the role of thermal notches in driving localised calving failure at Fjallsjökull.

5.2. Calving Failure and Localised Speed-ups

Thermal notches are integral to the calving process because they can undercut the terminus at the waterline, increasing the force imbalance in these localities and thus promoting calving failure (Benn and others, 2007; Mallalieu and others, 2020). As mentioned previously, three large calving events were observed in this study (one in 2019, two in 2021), with all three events occurring in the same part of the lower study region. Importantly, extensive thermal notches were observed at the waterline on both the 4 July 2019, and the 4 and 6 July 2021, within the same region where each of the three large calving events later occurred, strongly suggesting that these notches were the primary driver behind each event.

It was illustrated by Benn and others (2017) through discrete element modelling that thermal notch undercutting can be associated with two types of calving failure: (i) low-magnitude events that occur where loss of support by undercutting exacerbates existing faults in the ice cliff, causing small localised subaerial failures, and (ii) high-magnitude events which are associated with the propagation of suitably orientated surface crevasses and outward bending of the ice cliff over the undercut, leading to collapse of the entire column. Through analysis of the calving front before each event occurred, and based on the size of each event overall, the type of calving failure observed in both July 2019 and 2021 was most similar to mode (ii).

Before the July 2019 event, as well as the first event in July 2021, several large, suitably orientated crevasses were observed at the ice surface, in the same region where these calving events later occurred (Fig. 8). Importantly, many of these crevasses were also closely aligned to the precise failure surface of these events, and as a result we propose that the undercutting of the terminus via notch development increased the force imbalances acting on the terminal face, leading to a corresponding increase in the stresses acting on the ice surface, which promoted fracture propagation until full failure occurred (Benn and others, 2007; 2017). For the second event in 2021, although suitably orientated crevasses were again observed (Fig. 8c), these were not as extensive as for the other two events. In this case, we suggest that a combination of crevasse propagation, as well as the stress imbalance resulting from the loss of a large volume of ice <24 hours prior were the likely drivers for this event.

It is important to note that due to a lack of continuous observations, we cannot say with complete certainty that calving occurred as a single, high-magnitude event on each occasion. Rather, they may have been made up of several smaller calving events that occurred in quick succession. However, the presence of clear lines of weakness at the ice surface in both 2019 and 2021, and the fact that these crevasses closely correspond to the precise failure surface of these calving events, strongly suggests that they likely did occur as large, high-magnitude events.

Significantly, these calving events were also likely responsible for the localised increases in velocity that were observed in this region in both 2019 and 2021, particularly in the days that followed each individual event. Previous work at several tidewater glaciers in Greenland has demonstrated that the balance of glacier stresses which control the flow of calving glaciers are highly sensitive to any change in the position or thickness of the calving front (Howat and others, 2007; Nick and others, 2009). More specifically, any sudden changes in the position of the calving front, whether glacier-wide or localised (i.e., from high-magnitude calving) will cause a reduction in the resistive stresses due to the sudden loss of a large volume of ice (Joughin and others, 2008a; Howat and others, 2010; Murray and others, 2015). In response, the glacier speeds up and draws-down ice from higher elevations to provide the additional resistive stresses that are necessary to restore the stress balance (Howat and others, 2005; Joughin and others, 2008a). As a result, brief periods of calving activity and retreat, lasting days or less, can result in an acceleration of ice flow that is sustained over a much longer period as the glacier evolves following the perturbation at the front (Joughin and others, 2008b; Howat and others, 2010; Murray and others, 2015).

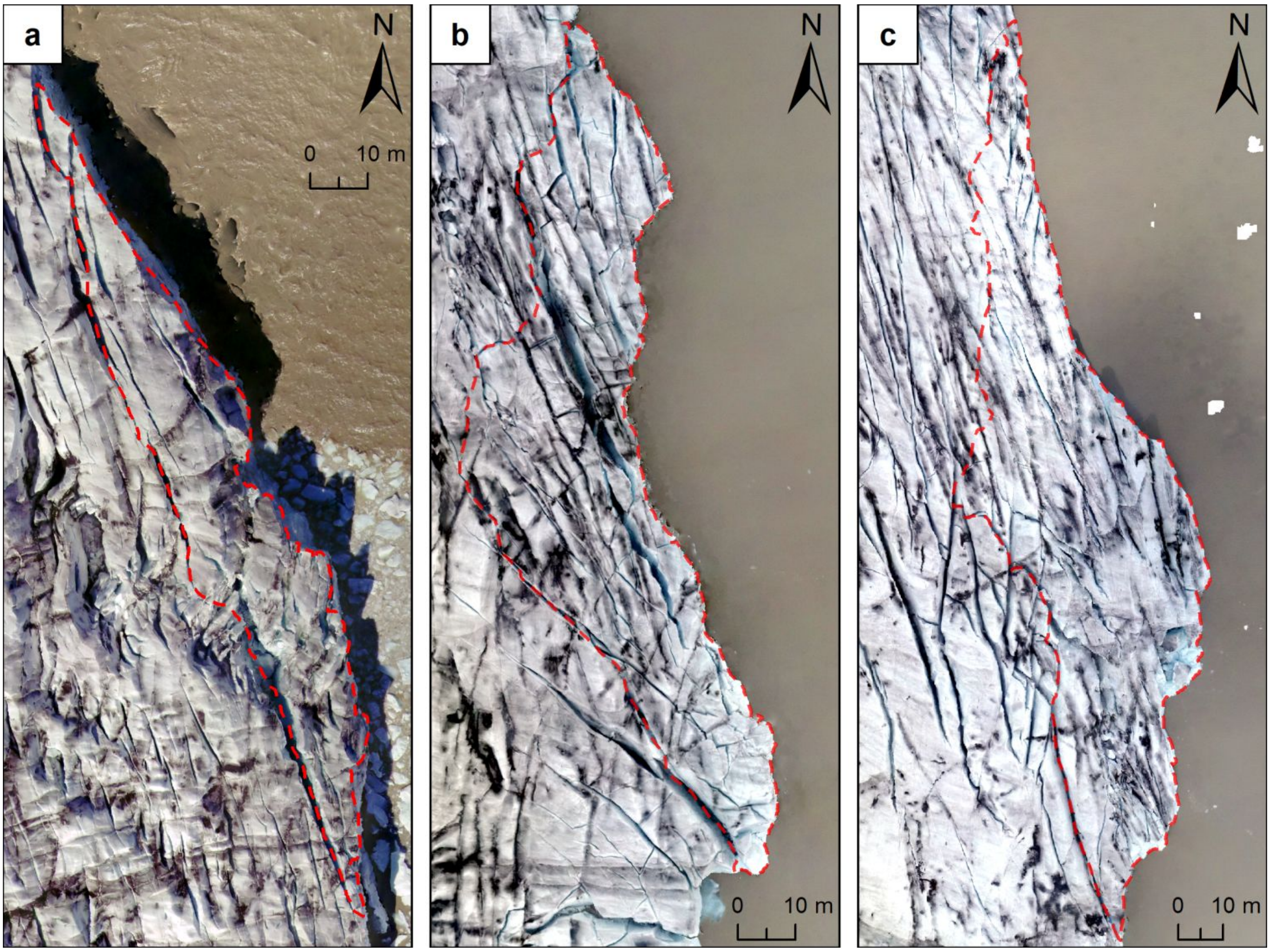

Fig. 8. Orthomosaics from (a) 5 July 2019, (b) 4 July 2021 and (c) 6 July 2021, illustrating the presence of suitably orientated crevasses at the ice surface in the same region where the large calving events described in-text later occurred. Dashed red lines in each panel highlight the area of ice that calved in each event. Note how these lines closely correspond to the location and orientation of the crevasses at the ice surface, indicating that calving occurred along these lines of weakness.

Although such a dynamic response has yet to be observed at a lake-terminating glacier in nature, and that there are notable differences between the processes occurring at tidewater glaciers in Greenland to those potentially underway here, we strongly believe that a similar set of processes may be occurring at Fjallsjökull, based on the data presented in this study. Indeed, localised speed-ups are clearly observed in our velocity data, and as a result we suggest the following sequence of events likely occurred in July 2021 (a similar sequence of events also occurred in this region in July 2019, but over a slightly shorter timescale):

i. The first calving event occurred between the 4 and 6 July, leading to locally high velocities (~0.72 m d^{-1}) in the region immediately behind the new position of the calving front, but with little change in velocity observed elsewhere.

ii. The second large calving event occurred over the following 24 hours, causing this region of locally high velocities to not only increase in areal extent, but to also increase in magnitude (to ~0.84 m d^{-1}). Consequently, it now extended some ~300 m back from the calving front (encompassing much of the lower study region as a result), as well as northwards, joining with the large region of high velocities in the upper portion of the study area. Such a change likely reflects the speed-up and drawdown of ice from further up-glacier in an attempt to restore the stress balance, following the sudden loss of a large volume of ice in a relatively short period of time.

iii. Over the following 48-hour period (7-9 July), although there was very little change in the overall extent of this region of elevated velocities, a further increase in peak velocity was observed during this time (to ~0.94 m d^{-1}), indicating how ice acceleration following calving failure can be sustained for several days after the initial event has taken place.

iv. It was only by the 11 July that velocities in this region had once again returned to their pre-speed-up magnitude and extent, ~five days after the initial calving event had occurred.

Such short-term increases in velocity, occurring over relatively large areas of the glacier in response to what were two large, but fundamentally localised, calving events, highlights the importance of thermal notch erosion as a key control on both calving losses (e.g., Röhl 2006; Minowa and others, 2017; Mallalieu and others, 2020) and localised ice dynamics.

There is the possibility that these speed-ups may have instead been forced by periods of relatively high air temperatures, which can cause calving glaciers to undergo short-term increases in velocity as a result of peaks in subglacial water pressure (e.g., Sugiyama and others, 2011; Doyle and others, 2018; Jouvet and others, 2018). However, we find it unlikely that increased air temperatures were the primary driver behind the observed speed-ups, for four reasons. Firstly, and perhaps most significantly, both speed-up events were initially only constrained to a small region in the immediate vicinity of the calving front (Fig. 5). If air temperatures were the primary driver, then we would expect this initial increase in velocity to occur over a much larger region of the glacier than is observed in our data.

Secondly, air temperatures were relatively low (Fig. 9) in the days preceding either of the speed-up events, with an average recorded temperature of ~10.6°C. It is unlikely, therefore, that these temperatures were sufficient to trigger the initial speed-up that was observed in both years. It could be argued that the 2019 event may have been driven by the relatively high temperatures recorded on the 5 July, which occurred <24 hours before the onset of this event (Fig. 9a). However, because the area that sped-up in this 24-hour period only initially encompassed a small region of the calving front strongly suggests that these relatively high temperatures were not the cause. Third, peak temperatures were only reached after the speed-up events had already begun, and while these high temperatures may have contributed to the duration of these events (particularly in 2021), as well as the overall magnitude of the velocity peaks observed in both years, their influence as a forcing mechanism for these events is clearly limited as a result.

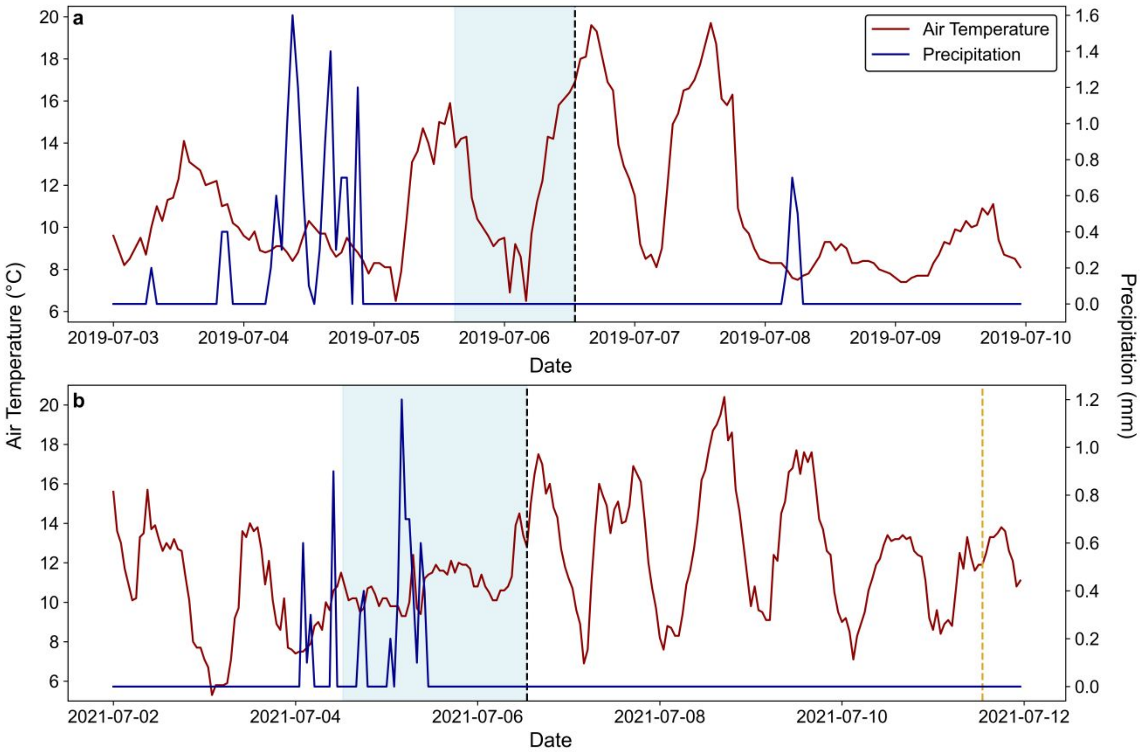

Fig. 9. Hourly air temperature and precipitation data for (a) July 2019 and (b) July 2021. Legend in (a) is shared between both plots. Vertical dashed black lines indicate the onset of the speed-up events in both years, based on our UAV-SfM data, whilst the blue shaded regions mark the period in which the large calving events are known to have occurred. Vertical dashed gold line in (b) indicates the end of the speed-up event in 2021, based on our UAV-SfM data. Data obtained by the Icelandic Met Office from their weather station at Kvísker (63°58'N, 16°26'W, ~30 m a.s.l.), located ~5 km to the south of Fjallsjökull.

Fourth, any increase in subglacial meltwater (from increased air temperatures) would need to leave the glacier front via a suitable discharge outlet (e.g., a meltwater plume), yet no obvious outlet or plume were observed in this region of the glacier in either year. Instead, field observations indicate that there are two main discharge outlets at Fjallsjökull: The first is situated towards the middle of the glacier front, within the main calving embayment, whilst the second is situated next to the southern grounded margin, near the lake shoreline: i.e., in two different regions of the glacier than where the speed-up events were observed. Importantly, neither of these outlets exhibited any increase in discharge prior to the onset of either speed-up event (based on our observations), and as a result we are confident that increased air temperatures, and concurrent peaks in subglacial discharge, can be ruled out as the primary driver of these events.

It is also important to note that due to the daily separation of our UAV-SfM surveys, we cannot state with complete certainty whether these speed-ups occurred in direct response to the large calving events. Instead, there is the possibility that these calving events may have occurred as a result of an increase in surface velocity. Nonetheless, if this was the case then it's unclear what the forcing mechanism could have been in the absence of calving. Indeed, as discussed previously we can already discount certain processes (e.g., periods of high air temperatures and increased meltwater discharge), although there are other potential forcing mechanisms.

For example, several previous studies have shown how intense periods of precipitation, totalling 10s mm in <24 hours, can cause calving glaciers to undergo rapid, but short-term (<24-48-hour) increases in velocity (e.g., Sugiyama and others, 2015; How and others, 2017). However, no precipitation fell in the 24-hours prior to the onset of the 2019 event (Fig. 9a), and although some precipitation did fall prior to the 2021 event, this only totalled ~4.7 mm (Fig. 9b), which is unlikely to have been sufficient to trigger the initial speed-up that occurred in this year. As a result, we can confidently discard intense periods of precipitation as a potential forcing mechanism. Similarly, variations in the level of the proglacial water body can also impact glacier velocity over short timescales (e.g., Kirkbride and Warren, 1997; Dykes and others, 2011). However, our field observations indicate that the level of Fjallsárlón changed very little across either study period, particularly before the onset of each speed-up event, suggesting that variations in lake level are also unlikely to be the primary cause.

In contrast, because these large calving events were observed in the same region of the glacier across both years, and because the resultant speed-ups were only limited initially to the area immediately surrounding where these individual events occurred, strongly suggests that these large calving events were the forcing mechanism, providing new insights into the dynamic behaviour of the glacier. To the best of our knowledge, we are the first study to demonstrate how these high-magnitude calving events, occurring as a direct result of thermal notches at the waterline, can drive short-term increases in velocity at a lake-terminating glacier.

Moreover, there is the potential that these processes could cause the glacier to undergo increased mass loss, through a repeat cycle of notch formation and calving. As we have demonstrated, the presence of extensive thermal notches at the waterline can drive high-magnitude calving. To replace these losses, the glacier speeds up, drawing down ice from further up-glacier, and in doing so, bringing more (new) ice close to the terminus. If new notches can then form and grow at the waterline over the space of several days, it is not inconceivable that these notches could also result in high-magnitude calving. Assuming the rate of notch erosion remains high, and that these notches can grow large enough in order to trigger these high-magnitude events, then this set of processes could occur repeatedly over an extended period of time, leading to increased mass loss. As a result, these processes may contribute an additional, yet at present, poorly quantified component of mass loss, with potential implications for the overall dynamics and stability of the glacier.

5.3. Wider Relevance and Future Outlook

It was previously suggested by Dell and others (2019) that calving at Fjallsjökull likely occurs via a combination of buoyant forces acting on the terminus, force imbalances at terminal ice cliffs and subaqueous melting, although they could not provide direct evidence for any of these processes occurring. However, our field observations from both July 2019 and July 2021 provide direct evidence that subaqueous melting is occurring at the terminus of Fjallsjökull, due to the presence of extensive thermal erosion notches at the waterline. Indeed, we demonstrate how these notches can form and grow relatively rapidly at the waterline, following calving. Furthermore, our data also indicate that these notches are likely driving high-magnitude calving in this region, based not only on the size of the observed events, but also from the evidence of extensive lines of weakness at the ice surface before these events occurred. Finally, and perhaps most significantly, we have shown that these large calving events can drive short-term increases in velocity, which are sustained for several days and occur over a much larger area of the glacier than was originally impacted by the initial event.

Our findings are likely to be important for other lake-terminating glaciers both in Iceland, and elsewhere, where extensive thermal notches have been observed previously (e.g., Dykes and others, 2011; Minowa and others, 2017; Mallalieu and others, 2020). However, our findings may also be applicable to several tidewater glaciers, for example in Svalbard, where calving is also known to be driven by extensive notch erosion at the waterline (e.g., Pętlicki and others, 2015; How and others, 2019). It is entirely plausible, therefore, that in both these settings high-magnitude calving could result in short-term increases in velocity, and potentially, increased mass loss. Yet despite extensive thermal notches being observed in these studies, and that these notches drive calving behaviour in these settings, none of these studies were able to observe the resultant short-term increases in velocity that we do here. Although this could be due to several different factors, we believe a combination of the specific methodology chosen by these studies, as well as how these studies have then employed these methods, to be the most important.

For example, time-lapse photography has become an increasingly popular method over recent years due to its ability to facilitate the generation of both short- (i.e., hourly-daily) and long- (i.e., seasonal-annual) term data sets of calving front dynamics at fine temporal resolutions (e.g., Medrzycka and others, 2015; Pętlicki and others, 2015; How and others, 2019; Mallalieu and others, 2020). Furthermore, when combined with SfM techniques, the method can allow for the extraction of calving volumes, permitting a more detailed analysis of the drivers of calving in these regions to be undertaken (e.g., Mallalieu and others, 2017; 2020).

However, whilst the method has been used previously to successfully generate surface velocity fields (e.g., Ahn and Box, 2010), in many studies the oblique angle at which images are captured can often lead to very high errors when attempting to derive measurements of surface velocity (e.g., Mallalieu and others, 2017; How and others, 2019). As a result, velocity measurements are often not undertaken, or are unfeasible. Therefore, although previous studies have successfully utilised this technique to acquire a continuous record of calving in both freshwater and tidewater environments (e.g., Medrzycka and others, 2015; How and others, 2019; Mallalieu and others, 2020), the specific camera set-up used in these studies has meant that any localised speed-ups which may have occurred in response to calving will not have been quantified.

More traditionally, much of our understanding of the calving patterns and overall dynamics of both freshwater and tidewater glaciers stems from the application of satellite remote sensing, which facilitates the monitoring of these glaciers over a range of spatial (glacier-wide to regional) and temporal (days to decadal) scales (e.g., King and others, 2018; Sakakibara and Sugiyama, 2018; Baurley and others, 2020). However, although the method has been previously used to successfully investigate the role of melt undercutting on calving rates (e.g., Luckman and others, 2015), in general the relatively coarse spatial and temporal resolution of this imagery means it can be difficult to monitor those processes occurring over fine spatial and temporal scales (Pętlicki and others, 2015; Mallalieu and others, 2017; Jouvet and others, 2018), such as the localised speed-up events observed here.

To explore this, we aggregated our UAV-SfM orthomosaics to the resolution of two of the most commonly used, and freely available satellite sensors, Planet and Sentinel-2, before recalculating the velocity based on the typical temporal baseline of these sensors. More specifically, we aggregated our July 2019 data to the resolution of Planet (Fig. S6), whilst our July 2021 data was aggregated to the resolution of both Planet and Sentinel-2, due to the longer period covered by this data (Fig. 10). However, because the data from the 4 July covered a smaller area than the subsequent survey days, it was omitted from this analysis to ensure fair comparison between the different data. As a result, the Sentinel-2 comparison only covered ~9 days, rather than the typical 12 for this sensor.

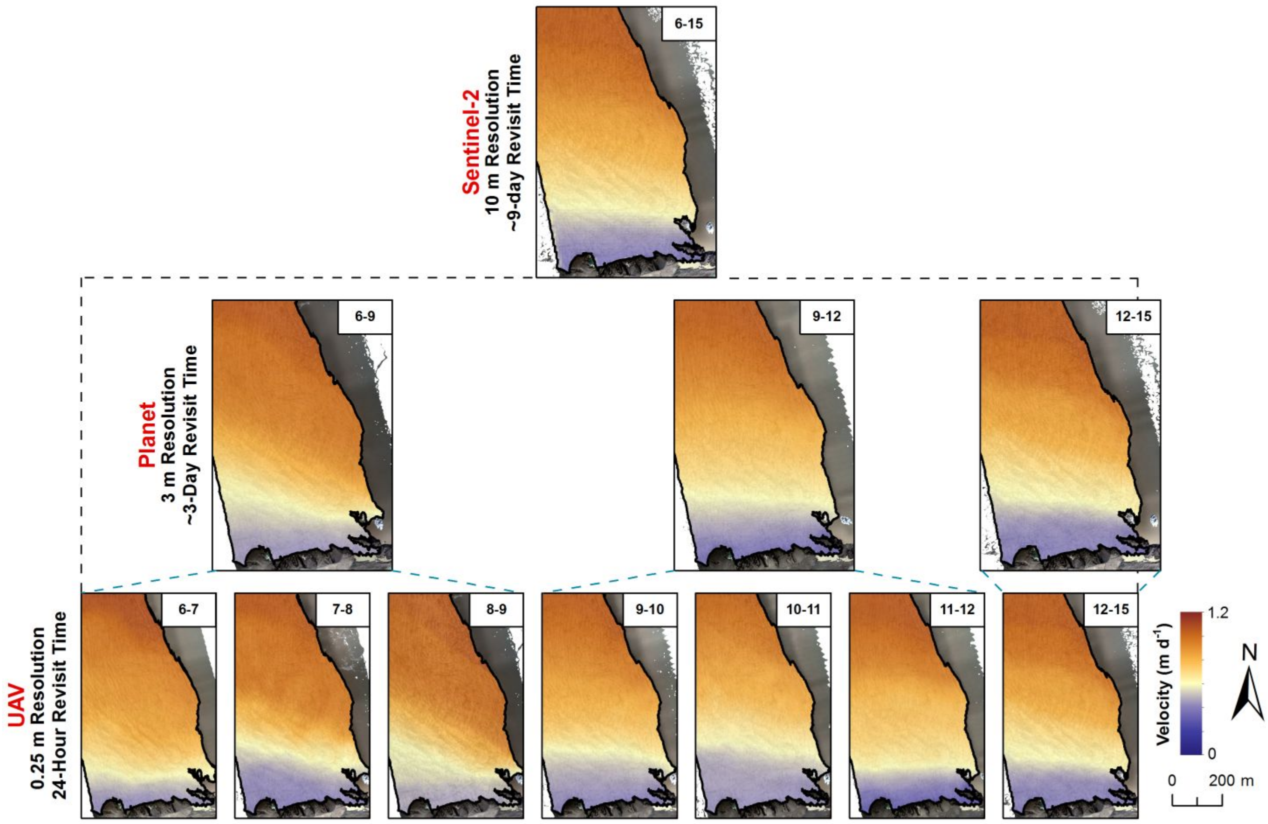

Fig. 10. Orthomosaics from July 2021, aggregated to the resolution of both Sentinel-2 and Planet imagery, before calculating the velocity based on the typical temporal separation of these sensors. These are displayed alongside the UAV-derived velocity grids to illustrate how the coarse spatial and temporal resolution of the satellite data make them unsuitable for the capture of the localised speed-up events observed in this study. Note that the Sentinel-2 comparison only covers ~9 days, rather than the typical 12, because the UAV-SfM data from the 4 July was omitted from this analysis. Background in each panel is the orthomosaic for the latter period.

Nevertheless, what this analysis importantly illustrates is that the day-to-day variations in velocity that are observed in the UAV-SfM data, which occur during both speed-up events, are much harder to discern in the two sets of aggregated data, but particularly the data aggregated to the resolution of Sentinel-2. For these data, the longer temporal baseline between image acquisitions has caused the day-to-day variations in velocity to be averaged out over the longer time period (~3 or ~9 days), causing these speed-up events to be missed (Nagler and others, 2015; Sugiyama and others, 2015). Furthermore, the high velocity gradients, as well as the overall magnitude of the velocity peaks observed in the UAV-SfM data, have also been missed in the aggregated outputs. This is because the spatial resolution of these data, being some 12 (Planet) and 40 (Sentinel-2) times coarser than the UAV-SfM data, has caused these high velocities to be smoothed over, masking their overall signal (Altena and Kääb, 2017; Rohner and others, 2019). As a result, it is impractical to use satellite data to monitor and analyse those localised speed-up events that may occur in response to high-magnitude calving.

In contrast, this study has illustrated how UAV-SfM is an effective and highly suitable tool for the capture and monitoring of these speed-up events, due to the high spatial and temporal resolution of the sensor. In particular, the "on demand" deployment of the UAV system meant that we were able to undertake surveys almost every day (weather permitting), allowing variations in ice velocity to be investigated at a temporal resolution that would be nearly impossible to obtain using more traditional techniques. Furthermore, although it was not specifically done here, it would have also been possible to undertake multiple surveys each day, which may have provided important additional insights into these speed-up events.

However, despite its ability to accurately capture and monitor these speed-up events, UAV-SfM importantly does not provide a continuous record of change. For example, while the method can be used to provide an estimation of the total amount of ice that calved between successive surveys (like done here), often the temporal resolution is still too coarse to be able to determine when exactly these calving events occurred, and consequently, whether these calving events do drive short-term increases in velocity. Yet, while we are confident that the speed-ups observed here did occur as a direct result of calving, additional work is clearly required.

In particular, we suggest future studies utilise a combination of both UAV-SfM surveys and terrestrial time-lapse photography in order to address the limitations described above, as well as to ensure the accurate determination of glacier velocity at high spatial and temporal scales. We also suggest that future studies employ these methods across a larger number of glaciers in both freshwater and tidewater settings in order to increase the number of high-resolution field observations from these environments. This would allow these processes, and in particular, these localised speed-up events, to be investigated in extremely high detail across a range of glaciated regions, providing valuable insights into the relative importance of these processes, not just for the dynamic behaviour of these glaciers, but also for their overall patterns of mass loss and stability, both at present and in the future.

6. CONCLUSION

In this study, we utilised repeat high-resolution UAV-SfM surveys, alongside terrestrial photography acquired in-situ, to investigate the role of thermal notch erosion in forcing localised calving failure and subsequent short-term increases in velocity at an actively calving lake-terminating glacier in southeast Iceland. This data was acquired daily (where possible) across one week in July 2019 and two weeks in July 2021 to provide insights into a suite of processes that are presently under-studied. We show that extensive thermal notches are present at the waterline in both years, and that the relative size of these features varies over time. We also illustrate how new notches can form and grow relatively rapidly at the waterline following calving (<24 hours), and although no direct measurements of notch erosion could be made here, based on the size of these features, and how rapidly they formed, it is not inconceivable that rates of ~0.5 m d^{-1} could be possible.

Importantly, we demonstrate that these notches are also likely driving high-magnitude calving in this region of the glacier, based not only on the size of the observed events (surface area >1000 m^2), but also from the evidence of extensive lines of weakness at the ice surface before these events occurred. Finally, and perhaps most significantly, we have shown that these large calving events can drive short-term increases in velocity, which are sustained for several days and occur over a much larger area of the glacier than was originally impacted by the initial event. In 2019, velocities were ~25% faster than the average, peaking ~24 hours after the initial calving event, before beginning to decrease. In 2021 velocities were ~30%

faster than the average, but due to the occurrence of two large calving events in the space of two days, velocities didn't peak until three days after the initial event. Velocities only then returned to their pre-speed-up magnitude two days later.

To the best of our knowledge, we are the first study to demonstrate how these high-magnitude calving events, occurring as a direct result of thermal notches at the waterline, can drive short-term increases in velocity at a lake-terminating glacier. Therefore, our findings present an important and previously undocumented aspect of calving glacier behaviour, which has the potential to occur in both freshwater and tidewater environments. However, due to a lack of similar high-resolution field studies in these environments, the relative importance of these processes remains unknown. As a result, we strongly suggest that future studies investigate the importance of these processes across a larger number of calving glaciers in both freshwater and tidewater settings, in order to better understand their dynamic behaviour and overall stability, both at present and in the future.

CONFLICT OF INTEREST STATEMENT

The authors declare that the research was conducted in the absence of any commercial or financial relationships that could be construed as a potential conflict of interest.

DATA AVAILABILITY STATEMENT

The datasets generated for this study can be found in the following repositories: https://doi.org/10.5281/zenodo.7105133 and https://doi.org/10.5281/zenodo.7111111.

AUTHOR CONTRIBUTIONS

NB and JH devised the study. NB undertook the fieldwork, processed and analysed the UAV data and wrote the draft version of the manuscript. Both authors contributed to the writing and editing of the final manuscript.

SUPPLEMENTARY MATERIAL

The supplementary material for this article can be found at:

ACKNOWLEGEMENTS

NB wishes to thank David Sutherland and Chris Tomsett for their assistance across the two field campaigns, as well as the Vatnajökull National Park for providing a research permit to allow these campaigns to be undertaken. NB acknowledges funding from several sources: The July 2019 field campaign was funded by a Postgraduate Research Award from the Royal Geographical Society (with IBG), whilst the July 2021 field campaign was funded by a Dudley Stamp Memorial Award (part of the Postgraduate Research Awards) from the Royal Geographical Society (with IBG), and an expedition grant from The Mount Everest Foundation.

REFERENCES

Agisoft LLC (2021) Agisoft Metashape User Manual: Professional edition, Version 1.7. [online]. Agisoft LLC. Available from: https://www.agisoft.com/downloads/user-manuals/ [Accessed: 23rd September 2021].

Altena B and Kääb A (2017) Glacier ice loss monitored through the Planet cubesat constellation. In *2017 9th International Workshop on the Analysis of Multitemporal Remote Sensing Images (MultiTemp)* (1–4), Brugge, Belgium. *IEEE*. (doi: 10.1109/Multi-Temp.2017.8035235)

Ahn Y and Box JE (2010) Glacier velocities from time-lapse photos: Technique development and first results from the Extreme Ice Survey (EIS) in Greenland. *J. Glaciol.*, **56**(198), 723–734. (doi: 10.3189/002214310793146313)

Bartholomaus TC, Larsen CF and O'Neel S (2013) Does calving matter? Evidence for significant submarine melt. *Earth Planet. Sci. Lett.*, **380**, 21–30. (doi: 10.1016/j.epsl.2013.08.014)

Bash EA, Moorman BJ and Gunther A (2018) Detecting short-term surface melt on an Arctic Glacier using UAV surveys. *Remote Sens.*, **10**(10), 1–17. (doi: 10.3390/rs10101547)

Baurley NR, Tomsett C and Hart JK (2022) Assessing UAV-based laser scanning for monitoring glacial processes and interactions at high spatial and temporal resolutions. *Front. Remote Sens.*, **3**, 1027065. (doi: 10.3389/frsen.2022.1027065)

Baurley NR, Robson BA and Hart JK (2020) Long-term impact of the proglacial lake Jökulsárlón on the flow velocity and stability of Breiðamerkurjökull glacier, Iceland. *Earth Surf. Process. Landf.*, **45**(11), 2647–2663. (doi: 10.1002/esp.4920)

Benn DI and Åström JA (2018) Calving glaciers and ice shelves. *Adv. Phys-X*, **3**(1), 1513819. (doi: 10.1080/23746149.2018.1513819)

Benn, DI and 7 others (2017) Melt-under-cutting and buoyancy driven calving from tidewater glaciers: new insights from discrete element and continuum model simulations. *J. Glaciol*., **63**(240), 691–702. (doi: 10.1017/jog.2017.41)

Benn DI, Warren CR and Mottram RH (2007) Calving processes and the dynamics of calving glaciers. *Earth-Sci. Rev.*, **82**(3-4), 143–179. (doi: 10.1016/j.earscirev.2007.02.002)

Carrivick JL, Tweed FS, Sutherland JL and Mallalieu J (2020) Toward numerical modelling of interactions between ice-marginal proglacial lakes and glaciers. *Front. Earth Sci.*, **8**, 577068. (doi: 10.3389/feart.2020.577068)

Chudley T, Christoffersen P, Doyle SH, Abellan A and Snooke N (2019) High accuracy UAV photogrammetry of ice sheet dynamics with no ground control. *Cryosphere*, **13**(3), 955–968. (doi: 10.5194/tc-13-955-2019)

Dell R, Carr R, Phillips E and Russell AJ (2019) Response of glacier flow and structure to proglacial lake development and climate at Fjallsjökull, south-east Iceland. *J. Glaciol.*, **65**(250), 321–336. (doi: 10.1017/jog.2019.18)

Diolaiuti G, Citterio M, Carnielli T, D'agata C, Kirkbride M and Smiraglia C (2006) Rates, processes and morphology of freshwater calving at Miage Glacier (Italian Alps). *Hydrol. Process.*, **20**(10), 2233–2244. (doi: 10.1002/hyp.6198)

Doyle, S and 7 others (2018) Physical conditions of fast glacier flow: 1. Measurements from boreholes drilled to the bed of store glacier, west Greenland. *J. Geophys. Res. Earth Surf.*, **123**, 324–348. (doi: 10.1002/2017JF004529)

Dykes RC, Brook MS, Robertson CM and Fuller IC (2011) Twenty-first century calving retreat of Tasman Glacier, Southern Alps, New Zealand. *Arct. Antarct. Alp. Res*., **43**(1), 1–10. (doi: 10.1657/1938-4246-43.1.1)

Ely JC, Graham C, Barr ID, Rea BR, Spagnolo M and Evans J (2017) Using UAV acquired photography and structure from motion techniques for studying glacier landforms: Application to the glacial flutes at Isfallsglaciären. *Earth Surf. Process. Landf.*, **42**(6), 877–888. (doi: 10.1002/esp.4044)

Evans DJ and Twigg DR (2002) The active temperate glacial landsystem: A model based on Breiðamerkurjökull and Fjallsjökull, Iceland. *Quat. Sci. Rev.*, **21**(20-22), 2143–2177. (doi: 10.1016/S0277-3791(02)00019-7)

Guðmundsson S, Björnsson H, Pálsson F, Magnússon E, Sæmundsson Þ and Jóhannesson T (2019) Terminus lakes on the south side of Vatnajökull ice cap, SE-Iceland. *Jökull*, **69**, 1–34.

Hannesdóttir H, Björnsson H, Pálsson F, Aðalgeirsdóttir G and Guðmundsson S (2015) Changes in the southeast Vatnajökull ice cap, Iceland, between ~1890 and 2010. *Cryosphere*, **9**(2), 565–585. (doi: 10.5194/tc-9-565-2015)

Haresign E and Warren CR (2005) Melt rates at calving termini: A study at Glaciar Leon, Chilean Patagonia. *Geol. Soc. Lond. Spec. Publ.*, **242**, 99–109. (doi: 10.1144/GSL.SP.2005.242.01.09)

Haug T, Kääb A and Skvarca P (2010) Monitoring ice shelf velocities from repeat MODIS and Landsat data-a method study on the Larsen C ice shelf, Antarctic Peninsula, and 10 other ice shelves around Antarctica. *Cryosphere*, **4**(2), 161–178. (doi: 10.5194/tc-4-161-2010)

Heid T and Kääb A (2012) Evaluation of existing image matching methods for deriving glacier surface displacements globally from optical satellite imagery. *Remote Sens. Environ.*, **118**, 339–355. (doi: 10.1016/j.rse.2011.11.024)

Höhle J and Höhle M (2009) Accuracy assessment of digital elevation models by means of robust statistical methods. *ISPRS J. Photogramm. Remote Sens.*, **64**(4), 398–406. (doi: 10.1016/j.isprsjprs.2009.02.003)

How, P and 8 others (2019) Calving controlled by melt-under-cutting: Detailed calving styles revealed through time-lapse observations. *Ann. Glaciol.*, **60**(78), 20–31. (doi: 10.1017/aog.2018.28)

How, P and 9 others (2017) Rapidly changing subglacial hydrological pathways at a tidewater glacier revealed through simultaneous observations of water pressure, supraglacial lakes, meltwater plumes and surface velocities. *Cryosphere*, **11**(6), 2691–2710. (doi: 10.5194/tc-11-2691-2017)

Howat IM, Box JE, Ahn Y, Herrington A and McFadden EM (2010) Seasonal variability in the dynamics of marine-terminating outlet glaciers in Greenland. *J. Glaciol.*, **56**(198), 601–613. (doi: 10.3189/002214310793146232)

Howat IM, Joughin I and Scambos TA (2007) Rapid changes in ice discharge from Greenland outlet glaciers. *Science*, **315**(5818), 1559–1561. (doi: 10.1126/science.1138478)

Howat IM, Joughin I, Tulaczyk S and Gogineni S (2005) Rapid retreat and acceleration of Helheim Glacier, east Greenland. *Geophys. Res. Lett.*, **32**, L22502. (doi:10.1029/2005gl024737)

Immerzeel, WW and 6 others (2014) High-resolution monitoring of Himalayan glacier dynamics using unmanned aerial vehicles. *Remote Sens. Environ.*, **150**, 93–103. (doi: 10.1016/j.rse.2014.04.025)

Joughin, I and 8 others (2008a) Ice-front variation and tidewater behaviour on Helheim and Kangerdlugssuaq Glaciers, Greenland. *J. Geophys. Res. Earth Surf.*, **113**(F1). (doi: 10.1029/2007JF000837)

Joughin, I and 7 others (2008b) Continued evolution of Jakobshavn Isbrae following its rapid speedup. *J. Geophys. Res. Earth Surf.*, **113**(F4). (doi: 10.1029/2008JF001023)

Jenkins A (2011) Convection-driven melting near the grounding lines of ice shelves and tidewater glaciers. *J. Phys. Oceanogr.*, **41**(12), 2279–2294. (doi: 10.1175/JPO-D-11-03.1Jouvet and others 2017)

Jouvet G, Weidmann Y, van Dongen E, Luethi M, Vieli A and Ryan J (2019) High-endurance UAV for monitoring calving glaciers: Application to the Inglefield Bredning and Eqip Sermia, Greenland. *Front. Earth Sci.*, **7**, 206. (doi: 10.3389/feart.2019.00206)

Jouvet, G and 6 others (2018) Short-lived ice speed-up and plume water flow captured by a VTOL UAV give insights into subglacial hydrological system of Bowdoin Glacier. *Remote Sens. Environ.*, **217**, 389-399. (doi: 10.1016/j.rse.2018.08.027)

King O, Dehecq A, Quincey D and Carrivick J (2018) Contrasting geometric and dynamic evolution of lake and land-terminating glaciers in the central Himalaya. *Glob. Planet. Change*, **167**, 46–60. (doi: 10.1016/j.gloplacha.2018.05.006)

Kirkbride M and Warren C (1997) Calving processes at a grounded ice cliff. *Ann. Glaciol.*, **24**,116–121. (doi: 10.3189/S0260305500012039)

Lague D, Brodu N and Leroux J (2013) Accurate 3D comparison of complex topography with terrestrial laser scanner: Application to the Rangitikei canyon (NZ). *ISPRS J. Photogramm. Remote Sens.*, **82**, 10–26. (doi: 10.1016/j.isprsjprs.2013.04.009)

Luckman, A and 5 others (2015) Calving rates at tidewater glaciers vary strongly with ocean temperature. *Nat. Commun.*, **6**, 8566. (doi: 10.1038/ncomms9566)

Magnússon E, Pálsson F, Björnsson H and Guðmundsson S (2012) Removing the ice cap of Öræfajökull central volcano, SE Iceland: Mapping and interpretation of bedrock topography, ice volumes, subglacial troughs and implications for hazards assessments. *Jökull*, **62**, 131–150.

Mallalieu J, Carrivick JL, Quincey DJ and Smith MW (2020). Calving seasonality associated with melt-undercutting and lake ice cover. *Geophys. Res. Lett.*, **47**, e2019GL086561. (doi: 10.1029/2019GL086561)

Mallalieu J, Carrivick JL, Quincey DJ, Smith MW and James WHM (2017) An integrated structure-from-motion and time-lapse technique for quantifying ice-margin dynamics. *J. Glaciol.,* **63**(242), 937–949. (doi: 10.1017/jog.2017.48)

Medrzycka D, Benn DI, Box JE, Copland L and Balog J (2016) Calving behavior at Rink Isbræ, West Greenland, from timelapse photos. *Arct. Antarct. Alp. Res.*, **48**(2), 263–277. (doi: 10.1657/AAAR0015-059)

Minowa M, Sugiyama S, Sakakibara D and Skvarca P (2017) Seasonal variations in ice-front position controlled by frontal ablation at Glaciar Perito Moreno, the Southern Patagonia Icefield. *Front. Earth Sci.*, **5**, 1. (doi: 10.3389/feart.2017.00001)

Murray, T and 9 others (2015) Dynamics of glacier calving at the ungrounded margin of Helheim Glacier, southeast Greenland. *J. Geophys. Res. Earth Surf.*, **120**, 964–982. (doi: 10.1002/2015jf003531)

Nagler T, Rott H, Hetzenecker M, Wuite J and Potin P (2015) The Sentinel-1 mission: New opportunities for ice sheet observations. *Remote Sens.*, **7**(7), 9371–9389. (doi: 10.3390/rs70709371)

Nick FM, Vieli A, Howat IM and Joughin I (2009) Large-scale changes in Greenland outlet glacier dynamics triggered at the terminus. *Nat. Geosci.*, **2**(2), 110–114. (doi: 10.1038/ngeo394)

O'Leary M and Christoffersen P (2013) Calving on tidewater glaciers amplified by submarine frontal melting. *Cryosphere*, **7**(1), 119–128. (doi: 10.5194/tc-7-119-2013)

Pętlicki M, Ciepły M, Jania JA, Promińska A and Kinnard C (2015) Calving of a tidewater glacier driven by melting at the waterline. *J. Glaciol.*, **61**(229), 851–863. (doi: 10.3189/2015JoG15J062)

Purdie H, Bealing P, Tidey E, Gomez C and Harrison J (2016) Bathymetric evolution of Tasman Glacier terminal lake, New Zealand, as determined by remote surveying techniques. *Glob. Planet. Change*, **147**, 1–11. (doi: 10.1016/j.gloplacha.2016.10.010)

Rignot E, Fenty I, Xu Y, Cai C and Kemp C (2015) Undercutting of marine-terminating glaciers in West Greenland. *Geophys. Res. Lett.*, **42**(14), 5909–5917. (doi: 10.1002/2015GL064236)

Robson BA, Nuth C, Nielsen PR, Girod, L, Hendrickx M and Dahl SO (2018) Spatial variability in patterns of glacier change across the Manaslu Range, Central Himalaya. *Front. Earth Sci.*, **6**, 12. (doi: 10.3389/feart.2018.00012)

Röhl K (2006) Thermo-erosional notch development at fresh-water-calving Tasman Glacier, New Zealand. *J. Glaciol.*, **52**, 203–213. (doi: 10.3189/172756506781828773)

Rohner C, Small D, Beutel J, Henke D, Lüthi MP and Vieli A (2019) Multisensor validation of tidewater glacier flow fields derived from synthetic aperture radar (SAR) intensity tracking. *Cryosphere*, **13**(11), 2953–2975. (doi: 10.5194/tc-13-2953-2019)

Rossini, M and 7 others (2018) Rapid melting dynamics of an alpine glacier with repeated UAV photogrammetry. *Geomorphology*, **304**, 159–172. (doi: 10.1016/j.geomorph.2017.12.039)

Ryan, JC and 7 others (2015) UAV photogrammetry and structure from motion to assess calving dynamics at Store Glacier, a large outlet draining the Greenland ice sheet. *Cryosphere*, **9**, 1–11. (doi: 10.5194/tc-9-1-2015)

Sakakibara D and Sugiyama S (2018) Ice front and flow speed variations of marine-terminating outlet glaciers along the coast of Prudhoe Land, northwestern Greenland. *J. Glaciol.*, **64**(244), 300–310. (doi: 10.1017/jog.2018.20)

Schild, KM and 9 others (2018) Glacier calving rates due to subglacial discharge, fjord circulation, and free convection. *J. Geophys. Res. Earth Surf.*, **123**, 2189–2204. (doi: 10.1029/2017JF004520)

Sugiyama S, Sakakibara D, Tsutaki S, Maruyama M and Sawagaki T (2015) Glacier dynamics near the calving front of Bowdoin Glacier, northwestern Greenland. *J. Glaciol.*, **61**(226), 223–232. (doi: 10.3189/2015JoG14J127)

Sugiyama, S and 7 others (2011) Ice speed of a calving glacier modulated by small fluctuations in basal water pressure. *Nat. Geosci.*, **4**(9), 597–600. (doi: 10.1038/ngeo1218)

Tomsett C and Leyland J (2021) Development and Testing of a UAV Laser Scanner and Multispectral Camera System for Eco-Geomorphic Applications. *Sensors*, **21**(22), 7719. (doi: 10.3390/s21227719)

Truffer M and Motyka RJ (2016) Where glaciers meet water: Subaqueous melt and its relevance to glaciers in various settings. *Rev. Geophys.*, **54**(1), 220–239. (doi: 10.1002/2015RG000494)

Westoby MJ, Brasington J, Glasser NF, Hambrey MJ and Reynolds JM (2012) 'Structure-from-Motion' photogrammetry: A low-cost, effective tool for geoscience applications. *Geomorphology*, **179**, 300–314. (doi: 10.1016/j.geomorph.2012.08.021)

Whitehead K, Moorman BJ and Hugenholtz CH (2013) Brief Communication: Low-cost, on-demand aerial photogrammetry for glaciological measurement. *Cryosphere*, **7**(6), 1879–1884. (doi: 10.5194/tc-7-1879-2013)

Wigmore O and Mark BG (2017) Monitoring tropical debris-covered glacier dynamics from high-resolution unmanned aerial vehicle photogrammetry, Cordillera Blanca, Peru. *Cryosphere*, **11**, 2463–2480. (doi: 10.5194/tc-11-2463-2017)

Xue Y, Jing Z, Kang S, He X and Li C (2021) Combining UAV and Landsat data to assess glacier changes on the central Tibetan Plateau. *J. Glaciol.*, **67**(265), 1–13. (doi: 10.1017/jog.2021.37)

Yang, W and 8 others (2020) Seasonal Dynamics of a Temperate Tibetan Glacier Revealed by High-Resolution UAV Photogrammetry and In Situ Measurements. *Remote Sens.*, **12**(15), 2389. (doi: 10.3390/rs12152389)